Seasonal variability of the permanent thermocline off northern Chile

Marcel Ramos,[1,2] Oscar Pizarro,[2,3,4] Luis Bravo,[2] and Boris Dewitte[5]

Received 27 January 2006; revised 27 March 2006; accepted 31 March 2006; published 11 May 2006.

[1] The seasonal cycle of the depth of several isotherms representative of the main thermocline near the western coast of South America shows important semiannual and annual components. Annual thermocline oscillations are mainly related to wind stress curl changes and, secondarily, to alongshore wind and the annual equatorial Kelvin wave. In contrast, the important semiannual component observed in hydrographic data off Peru and Chile is mainly of equatorial origin. Based on satellite sea level anomalies and Rossby wave theory, we show that the coastal seasonal signal –annual and semiannual– propagates seaward near 21°S in the form of long Rossby waves, which may modulate the thermocline depth several hundreds of kilometers offshore. **Citation:** Ramos, M., O. Pizarro, L. Bravo, and B. Dewitte (2006), Seasonal variability of the permanent thermocline off northern Chile, *Geophys. Res. Lett.*, *33*, L09608, doi:10.1029/2006GL025882.

1. Introduction

[2] Most of the studies about the impact of equatorial disturbances on the western coast of the Americas have focused on interannual and intraseasonal variability, whereas the energetic seasonal changes –annual and semiannual– have received limited attention. Still, *Pizarro et al.* [2002] showed that the large semiannual oscillations observed in the Peru-Chile Undercurrent were related to long Rossby waves (RW) originating from equatorial Kelvin waves (EKW) reaching the South American coast. As shown by currentmeter records near 30°S, semiannual variability seems to be a distinctive feature of the eastern South Pacific [*Shaffer et al.*, 1999], although its impact on the seasonal cycle of other oceanographic parameters remains unclear. Here, based on about 20 years of hydrographic data from northern Chile and satellite altimetry, we document the impact of annual and semiannual equatorial disturbances on the seasonal cycle of the thermocline off northern Chile. We centered our analysis at about 21°S since this region has the greatest hydrographic data density in both time and space off Chile [*Blanco et al.*, 2001]. Linear theory was used to support the interpretation of the propagating characteristics of the observed signal off the coast of Chile and to investigate the coherency with remote forcing originating from the equator.

2. Data and Methods

[3] We used data from 97 oceanographic cruises covering the northern region of Chile between 1981 and 1998. A relatively long-term oceanographic program has been maintained in this region due to the importance of its pelagic fisheries. We considered all the hydrographic data collected inside two grids of one degree of latitude centered at 21°S. The first grid (coastal box) extends from the coast to 40 km seaward and the second (oceanic box) from 100 to 200 km from the coast. We refer to these boxes as centered at 20 km and 150 km from the coast. In our analysis, only temperature data were considered because of large errors observed in salinity data. The depths of several isotherms in the coastal and oceanic boxes were then computed. In the following, we refer to the 15°C isotherm depth as Z15 and so on for the other isotherm depths. The seasonal cycle of the isotherm depths was estimated by fitting annual and semiannual harmonics using the least squares method. We tested the statistical significance of the amplitude of each harmonic by running a Monte Carlo test, randomly reordering the values in the time series and estimating new amplitudes for the harmonics. It is worth noting that *Blanco et al.* [2001] presented a detailed hydrographic climatology of this region, but it was based on three calendar month averages, which do not allow proper resolution of the important semiannual component.

[4] To extend the above analysis to a wider region along the western coast of South America, we used temperature data from the *Boyer et al.* [2005] climatology. Based on this data set, we computed the yearly signal of the depth of several isotherms in the grid points closest to the South American coast (between 10°S and 35°S) with depths greater than or equal to 700 m. These yearly signals were then analyzed using standard empirical orthogonal function (EOF) methods to obtain a dominant mode of variability of the thermocline along the coast. To evaluate the quality of this gridded data set in the region, we used the index provided by *Boyer et al.* [2005]. To analyze the seasonal variability of the thermocline farther offshore, we used information from an oceanographic mooring (STRATUS buoy) located near 20°S, 85°W. This mooring is operated by WHOI (Dr. Robert Weller) and includes a well-instrumented surface buoy and a line with current and temperature sensors in the upper 500 m [*Vallée et al.*, 2002]. We also used data from an Argo float (3900174) deployed in November 2003 near the WHOI mooring site (Figure 4c).

[5] Sea level height (SLH) anomalies were obtained from TOPEX/Poseidon, ERS, and Jason altimeters (TPEJ) combined data sets from October 1992 to January 2005. A longitude-time diagram of these anomalies was constructed

[1]Programa de Doctorado en Oceanografía, Departamento de Oceanografía, Universidad de Concepción, Concepción, Chile.
[2]Center for Oceanographic Research in the eastern South Pacific (COPAS), Universidad de Concepción, Concepción, Chile.
[3]Departamento de Geofísica, Universidad de Concepción, Chile.
[4]Also at Laboratorio PROFC, Universidad de Concepción, Chile.
[5]Laboratoire d'Etudes en Géophysique et Océanographie Spatiales, Institut de Recherche pour le Développement, CNES, Toulouse, France.

0094-8276/06/2006GL025882

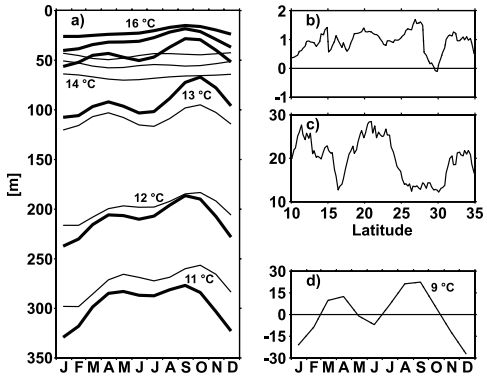

Figure 1. (a) Seasonal cycle of isotherm depths at 21°S, at 20 km (thick line) and 150 km (thin line) from the coast. (b) Alongshore structure of the first EOF mode for the seasonal Z9 cycle. The first mode EOF explains 62.3% of the yearly signal. (c) Coastal data quality index used for the EOF analysis (see text for further details). (d) First principal component of the seasonal Z9 cycle.

for 21°S. The zonal trend in the SLH data was subtracted to remove very long zonal scales of variability like those associated with seasonal thermal expansion. The annual cycle was determined by fitting annual and semiannual harmonics to the zonal and time detrended data.

3. Seasonal Variability of the Thermocline

[6] The depths of several isotherms (11°C to 16°C) laying in the upper 400 m were calculated from the original data in the coastal (20 km) and oceanic (150 km) grids centered at 21°S. We excluded the isotherms surpassing 500 m depth during any month since most hydrographic casts do not exceed that depth. Isotherms that reached the surface were also excluded from the analysis. Figure 1a shows the seasonal cycles for Z11 to Z16 in each grid. The depths of the shallower isotherms present weak seasonality, but Z11, Z12, and Z13 show a clear seasonal cycle where both annual and semiannual components are important. Shallower values of those isotherms were observed during April-May and September-October at both places, although Z11 and Z12 suggest a small lag between both locations, with the coastal isotherm leading. In the oceanic grid, annual and semiannual harmonics of Z11, Z12, and Z13, and annual harmonics of Z14 were significant at 95% confidence. Despite the relatively similar amplitude of the coastal seasonal cycle (as compared with the offshore seasonal cycle), neither annual nor semiannual harmonics were significant in the coastal grid. Note that the local Rossby radius for the first baroclinic mode is ~48 km, covering the coastal grid. There, large disturbances related to intraseasonal coastally trapped waves [e.g., *Pizarro et al.*, 1994; *Shaffer et al.*, 1997] can increase the variance of coastal time series, smearing the seasonal cycle. Even though these yearly signals near the coast are not statistically significant, their amplitudes and phases are realistic when compared with the seasonal cycles observed offshore. Below the upper thermocline the amplitude of the seasonal cycle of the isotherm depths increase rapidly downward. On the other hand, it is worth noting that the small cycle of Z14–Z16 tended to be opposite to the cycle presented by the deeper isotherms in the oceanic box, evidencing a possible effect of higher vertical modes near the surface.

[7] We selected Z9 (between 10°S and 35°S) to analyze the gridded data since this isotherm is representative of the main thermocline in the study region. The first EOF mode explains 62.3% of the yearly Z9 signal. In some coastal regions, where the quality of the gridded data is poor, the first principal component does not seem to represent seasonal variability (e.g., between 27° and 30°S) (Figures 1b and 1c). Despite these locations, the first EOF mode represents a significant fraction of the seasonal variability along the study zone. Furthermore, the estimated regional annual cycle is very similar to that observed at 21°S (Figure 1a). Apparently, the semiannual variability is a distinctive feature of the thermocline that extends from Peru to central Chile.

4. Offshore Propagation of Sea Level Disturbances

[8] Low-frequency fluctuations of the thermocline, like annual and semiannual disturbances, may propagate offshore as long RW at 21°S. That kind of propagation has been widely identified in different places using SLH anomalies [e.g., *Fu and Chelton*, 2001]. Figure 2a shows the longitude-time plot of SLH anomalies at 21°S from the South American coast to 110°W and from October 1992 to January 2005. The plot shows important spatial and temporal variability with clear patterns of diagonal stripes related to offshore propagation. *Vega et al.* [2003] used a similar SLH data set to study interannual RW related to El Niño-La Niña cycles. These authors found SLH disturbances that propagate offshore at about 5 cm s^{-1} at 27°S, about

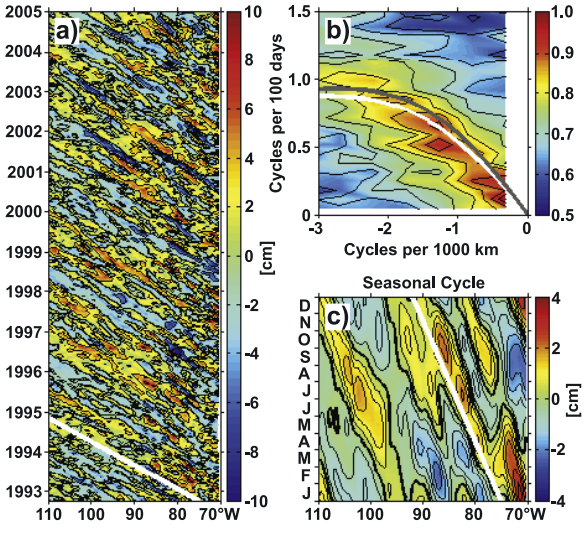

Figure 2. (a) Longitude-time diagram of the SLH anomalies at 21°S from TPEJ data. The white line represents the (standard) theoretical phase speed for the first vertical mode of a long RW. (b) 2-D spectrum for the data shown in Figure 2a. The thick lines in the spectrum are the dispersion curves for the standard theory (lower line) and the extended theory (upper line) for the first-mode baroclinic RW. (c) Longitude-time diagram of the seasonal cycle of SLH anomalies shown in Figure 2a.

30% larger than the theoretical phase speed for the long first-mode baroclinic RW. This difference between observed and theoretical speed has been widely recognized at subtropical latitudes and has been associated with the effect of a baroclinic mean flow that modifies the environmental vorticity gradient [e.g., *Fu and Chelton*, 2001]. The extended RW theory developed by *Killworth et al.* [1997] includes this effect by solving the linear quasi-geostrophic potential vorticity equation considering a vertically sheared mean zonal velocity. The mean baroclinic flow increases the meridional potential vorticity gradient by stretching the baroclinic vortex tube, thus increasing the restoring mechanism for RW. We use this theory to compute RW phase speed in the eastern south Pacific near 21°S. A geostrophic zonal velocity profile was estimated by using climatological temperature-salinity data from *Boyer et al.* [2005]. At this latitude, long RW phase speed is only slightly greater (∼13%) than the speed given by the standard theory. A comparison of both standard and extended RW theoretical dispersion curves are shown in Figure 2b. Most of the low frequency, large scale energy (from seasonal to interannual) is concentrated near the theoretical dispersion curve of the first-mode baroclinic RW. The above results suggest that an important fraction of the observed SLH anomalies are consistent with the propagation of RW, and they appear to be generated near the coast.

[9] The SLH seasonal cycle at 21°S also presents westward propagation, with a phase speed of 6.8 cm s^{-1}, estimated from the longitude-time diagram using a Radon transform [e.g., *Cipollini et al.*, 2000]; this speed is about 20% greater than the long first-mode baroclinic RW speed estimated from the standard theory (Figure 2c). Away from the coast, the semiannual harmonic makes a major contribution, although the annual harmonic seems to dominate near the coast. This result contrasts with the important semiannual signal observed in the thermocline depth near the coast (Figure 1a).

5. Data and Model Comparisons

[10] To investigate the forcing of the deep thermocline seasonal cycle and the dynamic contribution to the sea level variability, a multimode quasi-geostrophic model based on the simplified vorticity equation was used [c.f., *Vega et al.*, 2003]. The model was forced by the seasonal cycle of wind stress curl (calculated from five years of QuikScat satellite data) with a boundary condition for each mode imposed near the coast. This boundary condition was given from a low-frequency linear coastal model [*Clarke and Van Gorder*, 1994; *Pizarro et al.*, 2001] forced, in turn, by EKW and alongshore winds stress. A vertical mode decomposition was performed to derive the baroclinic mode contribution from the coastal model pressure perturbation in the deep ocean, about 110 km offshore. The first 2 modes were used to force the RW model (Figure 3c). A linear Rayleigh friction for each mode was included in the RW model. The decay times for modes 1 and 2 were 2.3 and 1.7 years, respectively. The phase velocity of the long first-mode baroclinic RW was obtained from the SLH seasonal cycle (Figure 2c). To estimate the second mode phase speed, we used the ratio between the phase speeds of mode 1 and 2, derived from the extended RW theory at 21°S. The EKW

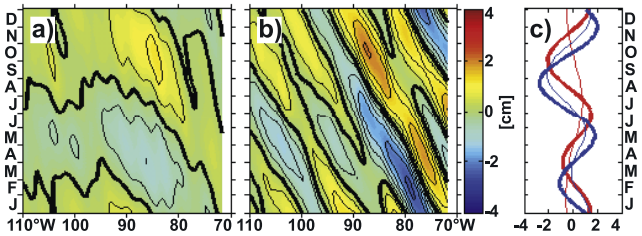

Figure 3. Simulated SLH seasonal cycle at 21°S using a linear RW model for the first 2 baroclinic modes. The model was forced with the regional wind stress curl using an eastern boundary condition obtained from a linear coastal model. The coastal model was forced with (a) alongshore wind stress and (b) alongshore wind stress and EKW. (c) Eastern boundary conditions (red lines) for the RW model derived from the coastal model, and sea level seasonal cycle from the EKW (blue lines) used to force the coastal model. First and second modes are indicated by thick and thin lines, respectively.

amplitude was estimated by using a linear model forced by zonal QuikScat wind stress along the equator, from 140°E to the South American coast [e.g., *Pizarro et al.*, 2002]. The RW model shows that the regional wind stress curl only contributes to the annual variability of the sea level (Figure 3a). In general, wind stress curl shows large annual and small semiannual amplitudes in the study region. In contrast, when the boundary condition is given by the coastal model, the RW presents a significant semiannual component with minimum values in March and October (Figure 3b). Note that the semiannual variability in the coastal model is due to the EKW. Near the South American coast, the semiannual amplitude of the mode 1 EKW is about twice the amplitude of the annual component, while for mode 2 both harmonics, annual and semiannual, have similar amplitude. On the other hand, a coastal simulation considering only alongshore wind stress did not show semiannual variability but only a small annual signal (sea level amplitude ∼1 cm).

[11] Temperature information from a deep ocean mooring located near 20°S and 85°W (Figure 4c) was used to evaluate the contribution that the signal originating at the coast made to the thermocline variability away from the coast. One year of temperature data (October 2000 to October 2001) was taken from *Vallée et al.* [2002]. Figure 4a shows the observed and simulated SLH anomalies, whereas Figure 4b shows observed and simulated isotherm variability at the mooring site. Note that a semiannual signal is present for both the observed and model sea levels. Isotherms between 8°C and 11°C, located below about 200 m, also present strong semiannual variability that is rather well correlated with the model signal at this place. Figure 4d shows the time variability of several isotherms from 900 m depth to the surface obtained from an Argo float drifting near the mooring site. During the first year of data, the variability of the lower isotherms in the thermocline (between 5°C and 11°C) fit rather well with the model seasonal cycle. As the buoy movement can be complicated, the interpretation of these data is not direct. Nevertheless, note that the float completed a year (Nov 2003 to Nov 2004) around relatively the same location, centered near 21°S and

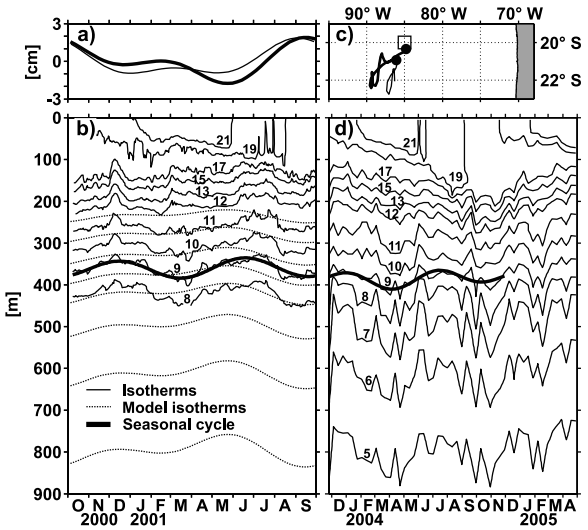

Figure 4. Comparison between model results and observed isotherms at 20°S and 85°W (STRATUS buoy) and along an Argo buoy path. (a) SHL seasonal cycle from TPEJ data (thin line) and sea level from RW model (thick line) near the STRATUS buoy location. (b) Observed Z8 to Z21 (thin line), model Z5 to Z12, and the 9°C isotherm seasonal cycle (thick line) at the STRATUS buoy. (c) The STRATUS buoy position (square) and the Argo buoy path (line). The circles show the release position of the drifting buoy and its position one year later. (d) Observed Z5 to Z21 (thin line) and seasonal cycle of the 9°C isotherm (thick line) from the Argo buoy. The seasonal cycle was calculated using only one year of data, without considering the large eddy present at the beginning of 2005.

87°30′W (Figure 4c). Both mooring and profiling buoy temperature variability also presented large high frequency variability, probably related to mesoscale eddies [e.g., *Chaigneau and Pizarro*, 2005]. Such eddies can strongly impact the seasonal cycle of the lower part of the thermocline, and longer time series are necessary to evaluate realistically low frequency variability in the region.

6. Summary and Conclusions

[12] Based on 20 years of hydrographic data from northern Chile (near 21°S), we showed that the lower part of the thermocline experiences significant semiannual variability in this region. Analysis of recently compiled global hydrographic climatology [*Boyer et al.*, 2005] revealed that this feature generally extends along most of the Peruvian and Chilean coasts. We explored the origin of this variability by analyzing the seasonal cycle of the alongshore wind stress and disturbances of equatorial origin using a linear coastal model. The alongshore wind stress near the coast was found to play a role in forcing the annual component of the seasonal cycle of the thermocline depth, but the important semiannual variability was associated with equatorial Kelvin waves reaching the South American coast. At these frequencies, the coastal signal propagates westward as long Rossby wave, contributing to the offshore semiannual cycle of the thermocline. The regional wind stress curl mainly contributes to the annual variability. Subsurface temperature from about 20°S, 85°W (~1500 km from the Chilean coast) showed a seasonal variability with an important semiannual component that is associated with the coastal signal and, in turn, with equatorial Kelvin waves. This variability is superimposed over the annual component forced mainly by the annual variability of the wind stress curl along the Rossby wave path.

[13] **Acknowledgments.** This work was supported by grants from the Chilean National Research Council (CONICYT, the FONDAP-COPAS Center, and FONDECYT Grant 1020294) and the Fundación Andes, Chile. M. Ramos was supported by a scholarship from CONICYT and a thesis scholarship (AT-4040200). Temperature data were obtained from SHOA-Chile, IFOP-Chile and NODC-USA; altimetry data from AVISO-CLS (France); and wind stress (QuikScat) from IFREMER (France). Supports from PBCT-Chile (Anillo project ACT-19) and ANR-France are also acknowledged. P. D. Killworth kindly provided us with the program to compute the RW vertical structure.

References

Blanco, J. L., A. C. Thomas, M. E. Carr, and P. T. Strub (2001), Seasonal climatology of hydrographic conditions in the upwelling region off northern Chile, *J. Geophys. Res.*, *106*, 11,451–11,467.

Boyer, T., S. Levitus, H. Garcia, R. Locarnini, C. Stephens, and J. Antonov (2005), Objective analyses of annual, seasonal, and monthly temperature and salinity for the World Ocean on a 0.25° grid, *Int. J. Climatol.*, *25*, 931–945.

Chaigneau, A., and O. Pizarro (2005), Eddy characteristics in the eastern South Pacific, *J. Geophys. Res.*, *110*, C06005, doi:10.1029/2004JC002815.

Cipollini, P., D. Cromwell, G. Quartly, and P. Challenor (2000), Remote sensing of oceanic extra-tropical Rossby waves, in *Satellites, Oceanography and Society*, edited by David Halpern, pp. 99–123, Elsevier, New York.

Clarke, A. J., and S. Van Gorder (1994), On ENSO coastal currents and sea level, *J. Phys. Oceanogr.*, *24*, 661–680.

Fu, L.-L., and D. B. Chelton (2001), Large-scale ocean circulation, in *Satellite Altimetry and Earth Sciences*, edited by L.-L. Fu and A. Cazenave, pp. 133–169, Academic Press, San Diego.

Killworth, P. D., D. B. Chelton, and R. A. de Szoeke (1997), The speed of observed and theoretical long extratropical planetary waves, *J. Phys. Oceanogr.*, *27*, 1946–1966.

Pizarro, O., S. Hormazabal, A. González, and E. Yañez (1994), Variabilidad del viento, nivel del mar y temperatura en la costa norte de Chile, *Invest. Mar. Chile*, *22*, 85–101.

Pizarro, O., A. J. Clarke, and S. V. Gorder (2001), El Niño sea level and currents along the South America coast: Comparison of observations with theory, *J. Phys. Oceanogr.*, *31*, 1891–1903.

Pizarro, O., G. Shaffer, B. Dewitte, and M. Ramos (2002), Dynamics of seasonal and interannual variability of the Peru-Chile Undercurrent, *Geophys. Res. Lett.*, *29*(12), 1581, doi:10.1029/2002GL014790.

Shaffer, G., O. Pizarro, L. Djurfeldt, S. Salinas, and J. Rutllant (1997), Circulation and low-frequency variability near the Chilean coast: Remotely forced fluctuations during the 1991–92 El Niño, *J. Phys. Oceanogr.*, *27*, 217–235.

Shaffer, G., S. Hormazabal, O. Pizarro, and S. Salinas (1999), Seasonal and interannual variability of currents and temperature off central Chile, *J. Geophys. Res.*, *104*, 29,951–29,962.

Vallée, C., K. Huang, and B. Weller (2002), Long-term evolution and coupling of the boundary layers in the Stratus Deck Regions of eastern Pacific (STRATUS) data report, *Tech. Rep. WHOI-2002–06*, 117 pp., Woods Hole Oceanogr. Inst., Woods Hole, Mass.

Vega, A., Y. du-Penhoat, B. Dewitte, and O. Pizarro (2003), Equatorial forcing of interannual Rossby waves in the eastern South Pacific, *Geophys. Res. Lett.*, *30*(5), 1197, doi:10.1029/2002GL015886.

L. Bravo, Center for Oceanographic Research in the eastern South Pacific (COPAS), Universidad de Concepción, Cabina 5, Casilla 160-C, Concepción, Chile. (lbravo@copas.udec.cl)

B. Dewitte, Laboratoire d'Etudes en Géophysique et Océanographie Spatiales, Institut de Recherche pour le Développement, CNES, 14 Av. Edouard Belin, F-31400 Toulouse, France. (boris.dewitte@legos.cnes.fr)

O. Pizarro, Departamento de Geofísica, Universidad de Concepción, Casilla 160-C, Concepción, Chile. (orpa@profc.udec.cl)

M. Ramos, Programa de Doctorado en Oceanografía, Departamento de Oceanografía, Universidad de Concepción, Casilla 160-C, Concepción, Chile. (mramos@profc.udec.cl)